Batteries & Supercaps

Research Article
doi.org/10.1002/batt.202400300

Chemistry Europe
European Chemical Societies Publishing

www.batteries-supercaps.org

Nickel Hexacyanoferrate as Cathode for Sodium-Ion Batteries: Effects of the Synthesis Conditions on the Material Properties

Victoria Carnero-Roldán,[a] Ángela Fernández-Merino,[a] Adrián Licari,[a] Giorgia Zampardi,[b] Fabio la Mantia,[b] and Rafael Trócoli*[a]

The increment in the energy demand and the limited availability of materials for manufacturing large-scale energy storage batteries based on Li-ion chemistry has increased the study of alternative technologies, including Na-ion batteries. The quest for superior electrochemical performances has led to the development new cathodes, such as Prussian blue and its analogs. Among the different members of this family of materials, $KNi[Fe(CN)_6]$ has attracted great attraction because of its low synthesis cost and excellent stability. Multiple synthesis approaches based on coprecipitation methods have been explored to optimize its capacity to intercalate sodium; however, the effects of the synthesis conditions on the structural and electrochemical properties of $KNi[Fe(CN)_6]$ remain vague. Therefore, in this work, we propose a detailed analysis of how the main synthesis parameters define the structural and electrochemical properties of $KNi[Fe(CN)_6]$.

Introduction

The fast expansion of the world's capacity to generate renewable electricity requires increasing energy storage capacities.[1,2] Currently, Li-ion batteries are the reference battery chemistry for most applications because of their high energy density, stability, and level of maturity, which are available on the market in multiple specifications. Yet, reducing the dependence on specific raw materials and adapting to the particular requirements of the diverse technologies that require efficient energy storage is essential since these not only demand improvements in key performance parameters such as power or lifetime but also at an economic and environmental level.[3–6] On the other hand, the forecast for future energy demand anticipates the need to develop new alternative batteries based on more abundant components.[7–13] Sodium-ion batteries have become of great interest due to their high safety, low cost, based on one of the most abundant elements, and excellent electrochemical properties; however, this technology has not yet reached the figure of merit of Li-ion batteries.[1,14] Studies of improved cathodes for these sodium batteries, still under development, show different possibilities, among which the intercalation of sodium cations in the material structure provides superior electrochemical performance with lower polarization and higher reversibility. In the quest for improved materials for Na batteries, compounds such as Prussian Blue (PB) have recently acquired essential relevance as cathodes for this battery technology.[14,15] Prussian Blue Analogues (PBAs) could be a low-cost alternative for their application as cathodes for sodium batteries since their low-temperature synthesis (25–80 °C), low-cost, e.g., common precursors are required for their synthesis (Sulfate/chloride/nitrate-based salts) – and low toxicity.[5] The open framework structure of PBAs (double perovskite, $A_xM[M'(CN_6)]_{y-\square}\cdot zH_2O$) consists of Fe atoms in the central position (M') linked by six cyanide bridges to M (Ni, Co, Mn…). The formal reduction/oxidation potential varies with the nature of the transition metal.[16–18] Na^+ or K^+ occupy the interstitial position A (Figure 1). This material may contain structural vacancies (Υ) caused by the absence of $[Fe(CN)_6]^{3-/4-}$ groups. H_2O molecules could occupy three positions: linked to the intercalated cations A, replacing the intercalated cation in

[a] V. Carnero-Roldán, Á. Fernández-Merino, A. Licari, R. Trócoli
Departamento de Química Inorgánica e Ingeniería Química, Instituto Químico para la Energía y el Medio Ambiente (IQUEMA), Facultad de Ciencias, Universidad de Córdoba, Campus de Rabanales, Córdoba 14071, Spain
E-mail: rafael.trocoli@uco.es

[b] G. Zampardi, F. la Mantia
Energiespeicher- und Energiewandlersysteme, Universität Bremen, Bibliothekstr. 1, Bremen 28359, Germany

Supporting information for this article is available on the WWW under https://doi.org/10.1002/batt.202400300

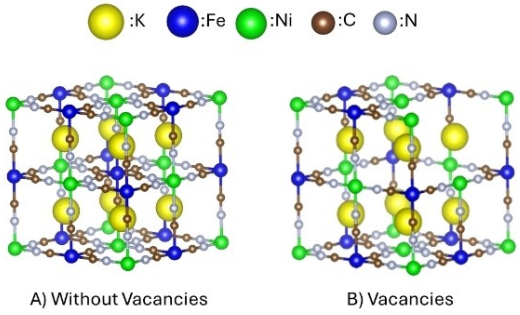

Figure 1. Cubic Prussian Blue Analogue structures (Fm-3 m) showing a perfect crystal (without vacancies) (A) and with two $[Fe(CN)_6]$ vacancies (B). For simplicity, water molecules are not shown.

Research Article
doi.org/10.1002/batt.202400300
Chemistry Europe
European Chemical Societies Publishing

the interstitial position A, or the vacancy (close to N position).[1,6,19]

PBAs have been extensively used as cathodes for sodium batteries.[20] Among the possible options, nickel hexacyanoferrate (NiHCF) has recently attracted significant attention because of its low synthesis cost, excellent electrochemical performance, and stability. The presence of vacancies in the structure (Figure 1B) affects the electrochemical behavior of the materials. Indeed, several authors have suggested potential superior electrochemical performances associated with low vacancy presence. Therefore, most studies have focused on controlling the number of vacancies, reducing their presence to minimum values, and trying to obtain defect-free structures.[6,21–23] Y. Xu et al. studied the so-called zero-vacancy $Na_{1.48}Ni[Fe(CN)_6]_{0.89}\cdot 2.87H_2O$, with 11% vacancies. The traditional coprecipitation method was modified by adding sodium pyrophosphate as a chelating precursor, controlling crystallization and defects formation.[1] Peng et al. proposed a hydrothermal post-treatment method to obtain a free of defects NiHCF with composition $Na_{1.64}Ni[Fe(CN)_6]_{0.92}\cdot 1.83H_2O$ – 8% of vacancies.[24] Both materials showed outstanding electrochemical performances in 1.0 M $NaClO_4$ in ethylene carbonate/dimethyl carbonate (1 : 1 vol) with fluorinated ethylene carbonate (2, 5%) as the electrolytes, reaching nearly 80 mAh/g. Besides reducing the number of vacancies, multiple strategies have been employed to optimize the PBAs, like reducing particle size, coating particles, creating singular morphologies or trying to avoid the formation of agglomerates.[22–24] However, there is no specific study focused on how the synthesis conditions govern the structural and electrochemical properties of this material. Therefore, we have analyzed here the effects that the synthesis parameters cause on the structural (morphological, compositional, and crystal symmetry) and electrochemical properties of a series of NiHCF compounds obtained by modifying critical synthesis parameters like concentrations and nature of precursors, their order of addition or the coprecipitation drip flow rate. We believe this study will pave the way for better design of Prussian Blue Analogues as insertion cathodes for sodium-ion batteries.

Table 1. Key parameters modified to synthesize $K_xNi[Fe(CN)_6]_y\cdot zH_2O$. NiHCF-0 refers to the initial synthesis conditions; just the parameters modified for the other synthesis concerning this procedure are included in the table. The column "order" refers to the addition of precursors. H_2O indicates that both precursors were dropped into a solution of 60 ml of water. Fe/Ni and Ni/Fe mean Fe- or Ni-based precursors were added to the Ni- or Fe-based precursor, respectively. EDTA = (Ethylenedinitrilo)tetraacetic Acid.

Sample	Precursor A	Precursor B	Order	Drip rate ml/min
NiHCF-0	0.1 M $NiSO_4$	0.1 M $K_4Fe[(CN)_6]$	H_2O	7.6
NiHCF-1	+ 1 M KCl			
NiHCF-2		0.5 M $K_4Fe[(CN)_6]$		
NiHCF-3	0.5 M $NiSO_4$			
NiHCF-4				19.4
NiHCF-5	+ 1 M KCl			0.4
NiHCF-6	+ 1 M KCl		Fe/Ni	
NiHCF-7	+ 1 M KCl		Ni/Fe	
NiHCF-8	+ 0.08 M EDTA			0.4
NiHCF-9	+ 0.08 M EDTA + 1 M KCl			0.4
NiHCF-10	+ 1 M KCl + 0.1 M $K_3C_6H_5O_7$			0.4

Results and Discussion

A detailed description of the synthesis method for NiHCF samples based on potassium hexacyanoferrate (III) (the absence of Na^+ in the synthesis solution provided less agglomerate and lower particles)[25] is included in the Experimental Section. Figure 2 briefly describes the synthesis procedure for preparing PBAs using a coprecipitation method. Critical synthesis conditions were modified to analyze their effects on the materials' properties.

Table 1 summarizes such modifications, indicating just the parameters modified in each synthesis respect the benchmark material, NiHCF-0; for example, NiHCF-1 was obtained by an equivalent method to NiHCF-0, yet adding 1 M KCl to the precursor A solution and, maintaining the rest of the synthesis parameters. One parameter was modified for each synthesis, allowing us to analyze how such parameters affect the material properties. The compositions of the synthesized materials (Table 2) were obtained by a combination of X-ray Fluorescence

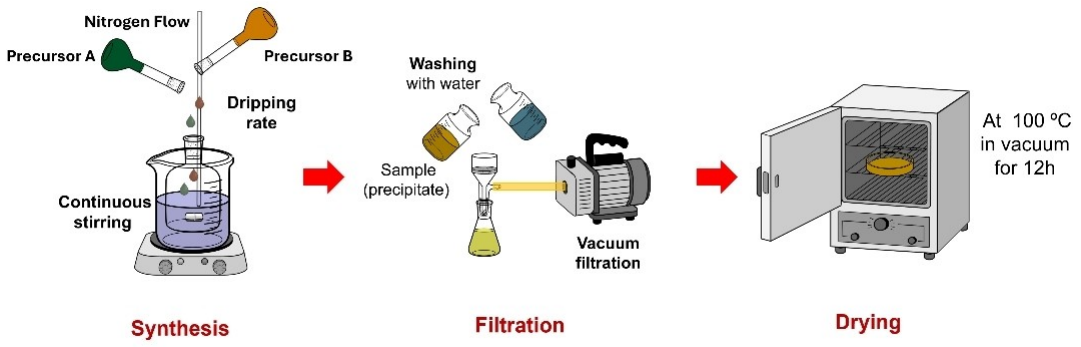

Figure 2. Schematic representation of the synthesis procedure of NiHCF materials. Variations of the synthesis procedure are collected in Table 1.

Table 2. Molecular composition of synthesized $K_xNi[Fe(CN)_6]_y \cdot zH_2O$ and theoretical capacity of each sample.

Sample	Molecular Composition	Theoretical capacity (mAh/g)
NiHCF-0	$K_{0.18}Ni[Fe(CN)_6]_{0.75} \cdot 4.45\ H_2O$	66.2
NiHCF-1	$K_{0.32}Ni[Fe(CN)_6]_{0.8} \cdot 4.2\ H_2O$	67.5
NiHCF-2	$K_{0.65}Ni[Fe(CN)_6]_{0.87} \cdot 4.3\ H_2O$	67.3
NiHCF-3	$K_xNi_x[Fe(CN)_6]_y \cdot zH_2O$	–
NiHCF-4	$K_{0.17}Ni[Fe(CN)_6]_{0.70} \cdot 4.9\ H_2O$	62.3
NiHCF-5	$K_{0.24}Ni[Fe(CN)_6]_{0.72} \cdot 5\ H_2O$	62.3
NiHCF-6	$K_{0.25}Ni[Fe(CN)_6]_{0.76} \cdot 4\ H_2O$	67.3
NiHCF-7	$K_{0.29}Ni[Fe(CN)_6]_{0.74} \cdot 4.6\ H_2O$	64.2
NiHCF-8	$K_{0.29}Ni[Fe(CN)_6]_{0.73} \cdot 2.5\ H_2O$	73.0
NiHCF-9	$K_{0.68}Ni[Fe(CN)_6]_{0.89} \cdot 2.2\ H_2O$	76.0

(*XRF*, Table S.1. sup.) and ATG measurements (Figure S.1). The theoretical Capacity, calculated based on the maximum number of electrons involved in the reaction, which is equivalent to the Fe content, was also included. The lower number of vacancies and water presence would cause the highest theoretical capacity – close to 76 mAh/g (sample NiHCF-9). The values for NiHCF-10 were not included because this synthesis route failed to obtain any precipitated material; no powder was recovered during the filtration step, probably because the citrate precursor fully complexed the Ni.

Moreover, the molecular formula and theoretical Capacity of NiHCF-3 could not be calculated since the material obtained following this procedure was based on the $Ni_xNi[Fe(CN)_6]_y$ composition. Calculating the "y" value, the number of ferrocyanide groups, required the normalization of the Fe content by the Ni value; vacancies are always attributed to $Fe(CN)_6$] losses, which implies that all the Ni occupy the M position. For $Ni_xNi[Fe(CN)_6]_y$, this premise is not fulfilled, hindering a proper calculation of the material composition.

The XRD diffractograms and the Rietveld refinements of the samples are shown in Figure 3, confirming the cubic symmetry (Fm-3 m) of all the materials (Figure 1). Cell parameters are included in Table S2. As mentioned above, all the samples showed XRD patterns equivalent to KNiHCF structures except for sample NiHCF-3, which showed a NiNiHCF diffraction pattern (Figure S2).[26] The comparison of all nine samples synthesized could be arduous, and the establishment of a direct relation between samples with multiple synthesis parameters is difficult; therefore, in the following section, we have divided the study comparing synthesis procedures with one parameter modified, allowing establishing a direct relation between this variation and the material properties. Figure 3 gathers all these comparisons, showing the differences observed in the XRD patterns and SEM images. Samples NiHCF-0 and NiHCF-1 (Figure 3A) allowed analyzing the effect of adding 1 M KCl solution to precursor A. Unlike what was reported in the literature,[21] where the addition of KCl to the synthesis procedure caused the synthesis of a material with higher crystallinity, a reduced number of vacancies, and lower agglomeration, we just observed how the introduction of KCl reduced the aggregation of the particles. However, we did not observe any substantial change in the XRD diffractogram (the cell parameters increased from 10.2274(2) to 10.2358(6)) or morphology, and minor variations in the composition were quantified (Table 2). Flow rate could also play a critical role in the structural and electrochemical properties of PBAs, as L. Zhang et al. demonstrated for ZnHCF as a cathode for Zn-ion batteries.[27] Increasing the flow from 7.6 ml/min (NiHCF-0) to 19.39 ml/min (NiHCF-4) caused a small reduction of crystallinity in the sample with faster precursors addition, showing slightly wider peaks and more vacancies, as well as smaller particles that stuck together, forming large agglomerations (Figure 3C). When the flow rate was reduced from 7.6 ml/min (NiHCF-1) to 0.4 ml/min (NiHCF-5) in the presence of KCl (Figure 3D), minor changes in XRD patterns were observed (the cell parameters increased from 10.2358(6) to 10.2264(3)). However, unlike the classic behavior observed for samples 0 and 4, the vacancy presence increased from 20% to 28%, and the presence of water increased from ≈4.2 to ≈5 molecules. On the contrary, the morphology varied following the expected behavior, obtaining larger particles upon flow reduction. This comparison demonstrates the complexity of PBAs synthesis; the presence of KCl, summed to a lower drip rate, instead of having a synergetic effect, higher particle size but lower vacancy presence, does not follow a linear trend. Unlike these relatively small changes, the concentration of the precursors had a tremendous impact on the materials obtained. Three different stoichiometries were analyzed: ratios of $NiSO_4$:$K_4Fe(CN)_6$ precursors equal to 1:1, 1:5, and 5:1 were studied (samples NiHCF-0, NiHCF-2, and NiHCF-3, respectively). As we mentioned above, the ratio 1:5 caused the formation of a $Ni_xNi[Fe(CN)_6]_y$-based material instead of $K_xNi[Fe(CN)_6]_y$, whose main characteristic in the XRD profile is a shift toward higher angles (Figure S2). This crystal structure was confirmed by the quantification of the cations composition, obtaining a Ni/Fe ratio of ≈1.7, between the $Ni_2[Fe(CN)_6]$ and $Ni_3[Fe(CN)_6]_2$ compositions, probably because K^+ was also found in the material.[28,29] The ratio of 5:1, an increment of the $K_4Fe[(CN)_6]$ concentration from 0.1 M to 0.5, caused a reduction of 16% in the number of vacancies and an increment in the K^+ content of 380%, both parameters, potassium content, and vacancies, are usually correlated since a lower number of vacancies implies more negative charges, which have to be compensated by K^+. Such variations did not result in a higher crystallinity, showing broader peaks than sample NiHCF-0. However, it caused a notorious enlargement of the cell parameter, from 10.2274(2) to 10.2560(9), and larger particle sizes were obtained, probably because the excess of Fe improves the particle nucleation (Figure 3B).

Another synthesis parameter potentially affecting the NiHCF properties is the order of precursor addition. Three options were explored: simultaneous dropwise addition of both precursors into the water, indicated in table one as the "H_2O" option (NiHCF-1), adding Fe-based precursor into Ni-based (NiHCF-6), and the contrary order, Ni into Fe (NiHCF-7). Modifying the precursor addition procedure also involves a variation in the concentrations of the cations. For sample

Research Article
doi.org/10.1002/batt.202400300
Chemistry Europe
European Chemical Societies Publishing

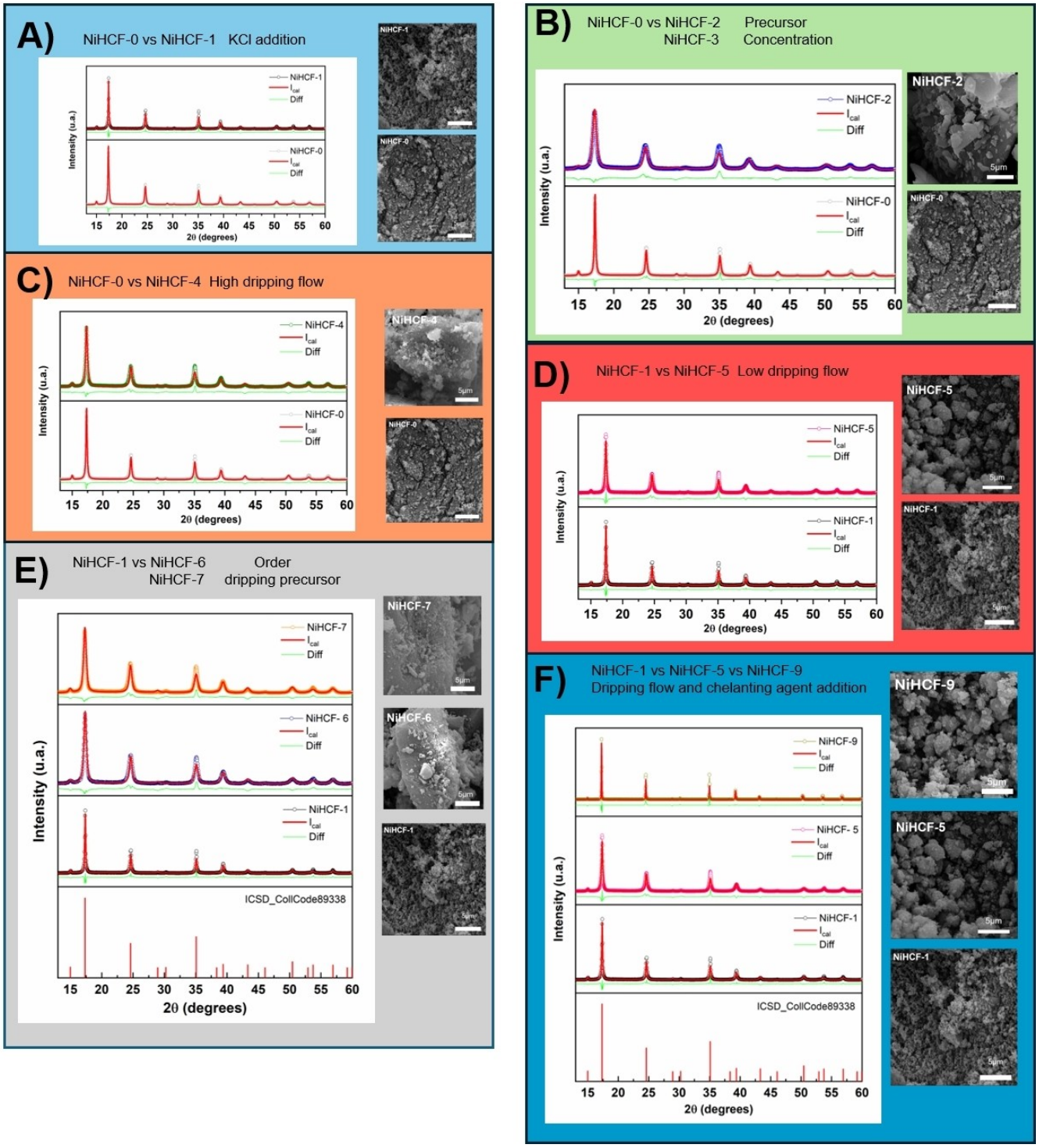

Figure 3. X-ray diffractograms and SEM images for all synthesized samples. The results are divided into groups comparing one or two synthesis parameters: A) Effect of KCl addition, B) Precursor concentration, C) High dripping flow, D) Low dripping flow, E) Order dripping precursor, and F) Dripping flow and chelating agent addition. Pattern KNiHCF(ICSD_CollCode89338).[26] Details of parameter changes are collected in Table 1.[30]

NiHCF-1, both precursors were dropped into 60 ml of water, and the Ni and Fe concentrations were low and remained relatively constant during the whole addition; however, the initial concentrations of Fe or Ni in samples NiHCF-6 and NiHCF-7 (0.1 M) are much larger than at the end of the addition, theoretically down to 0.038 M since the reactants were consumed during the addition. Lower concentrations could cause slower nucleation, improved crystallinity, and larger particle sizes.[30] However, the different addition methods caused minimal variations in the samples' compositions (Table 2) or the XRD pattern (Figure 3E, table S2). On the

contrary, the SEM images revealed an increment in particle size, especially for sample NiHCF-6.

Finally, using chelating agents as precursors has attracted significant attention as a method to reduce the nucleation rate, improve the crystallinity of the PBAs, and pursue low vacancy levels.[18,29,31–33] Such an approach was proposed in the seventies, using citrate.[32] Here, we analyzed the effect of adding EDTA as a precursor because of its superior capacity to form a Ni-based complex than citrate ($\approx 10^{13}$ times higher).[34] Furthermore, KCl, plus chelating-based synthesis, is also found in the literature.[17,23] Comparing NiHCF-5 (without) and NiHCF-9 (with EDTA) allows for studying the effect of adding EDTA to the synthesis procedure. The addition of the chelating agent reduced the vacancy level (Table 2) from 28% to 11% and the water content down to 2.2 molecules; however, when KCl was not included as a precursor (NiHCF-9), the vacancy level remained unchanged, suggesting a synergetic effect by combining EDTA and KCl. NiHCF-9 showed the sharpest diffraction peaks, yet minimal cell parameter changes, and the particles presented a cube-shaped morphology associated with excellent material crystallization and slow nucleation.[35]

Despite using the same Fe precursor, the synthesis method also affected the "apparent oxidation state" of the iron in the $K_xNi[Fe(CN)_6]_y$ electrodes. Figure 4 shows the first electrochemical cycle of the synthesized samples and the "apparent oxidation state" calculated based on the capacity delivered during the first oxidation. This "apparent oxidation state" does not refer to the real Fe oxidation state in the material yet to the

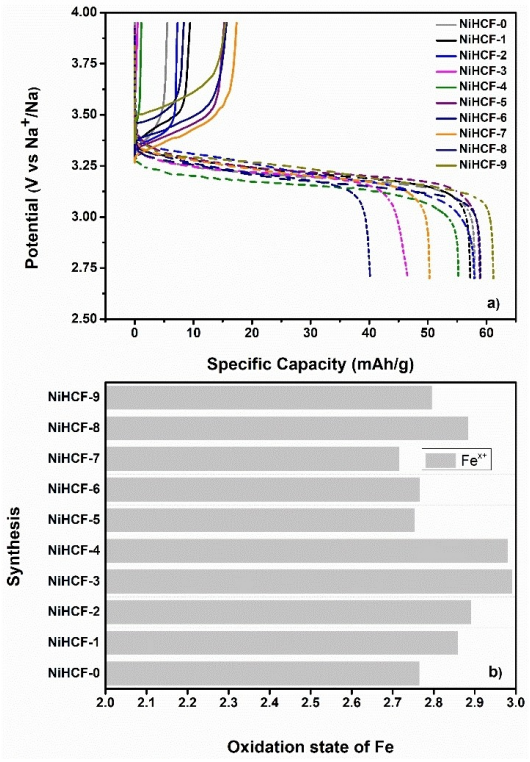

Figure 4. The first electrochemical cycle of synthesized samples a) and "apparent oxidation state" of Fe calculated from the capacity delivered in the first oxidation b).

% of Fe, which could contribute to the electrochemical performance if the cycling starts upon oxidation. Samples NiCHF-3 and NiHCF-4 showed an "apparent oxidation state" of Fe close to the value in the precursor (+3) since the initial oxidation capacity was minimal. On the contrary, other synthesis routes like NiHCF-0 and NiHCF-7 showed a reduction of the Fe "apparent oxidation state" close to 30%, indicating the existence of a reduction phenomenon. Different mechanisms could contribute to this reduction, including the decomposition of the $[Fe(CN)_6]^{3-}$ group[13] during the synthesis process or the self-discharge of the battery assembled, which is affected by multiple material-based parameters like particle sizes or porosity.[36–39]

The effects of the synthesis conditions on the electrochemical performances of the synthesized NiHCF were analyzed by a C-rate study in 1 M $NaClO_4$ EC: PC electrolyte. Like the previous methodology for comparing the structural properties, Figure 5 shows the electrochemical results gathered by samples with the minimum possible difference in the synthesis procedure.

Samples NiHCF-0 and NiHCF-1 (addition KCl, Figure 5A) provided similar capacities at slow C-rate, close to 55 mAh/g, equivalent to 82%–83% of their theoretical values; however, upon increment of the current rate, the capacity delivered by NiHCF-0 was considerably lower than for NiHCF-1, showing also a higher polarization (Figure S.3). Such discrepancies could be attributed to the more significant agglomeration of particles observed for NiHCF-0, which limits the kinetics of the material. Increasing the flow rate from medium (NiHCF-0) to high (NiHCF-4, Figure 5C and S.4 a and b) caused a reduction in the capacity provided, especially at 1 C, probably because of the lower content of vacancy presence in the sample at a low flow rate. In the same way, when the flow was further reduced to a low value in the presence of KCl (0.4 ml/min, NiHCF-5 vs. NiHCF-1, Figure 5C), superior performance of the sample obtained at low flow was obtained, providing 36% higher Capacity at C rate (Figure S.4 c and d), besides the in principle inferior material properties (higher particle size and levels of vacancies and water). The reason behind this unusual electrochemical behavior is not clear. It could be attributed to multiple causes, such as vacancy amount and distribution, the electrostatic shielding effect because of the higher water content, and different octahedral tilting. Further studies would be necessary to understand this behavior fully. On the other hand, as was observed for the structural properties, the concentration of the precursors had a tremendous impact on the electrochemical performance. The $K_xNi_{x'N}[Fe(CN)_6]_y$-based material showed the poorest electrochemical behavior, providing around 35 mAh/g at low C-rates and zero electrochemical response at faster currents (Figure 5B, S.5). On the contrary, the ratio $NiSO_4$:$K_4Fe(CN)_6$ equal to 5:1 (NiHCF-2) showed excellent electrochemical performance, with minimal capacity fading and polarizations upon C-rate increment because of the low presence of vacancies in this sample, equivalent to the amount reported for fast sodium intercalation PBA cathodes, which, unlike the material obtained in this study, showed a distortion from traditional face-centered cubic structure to monoclinic or rhombohedral symmetries.[1,24,31,34]

Research Article
doi.org/10.1002/batt.202400300
Chemistry Europe
European Chemical Societies Publishing

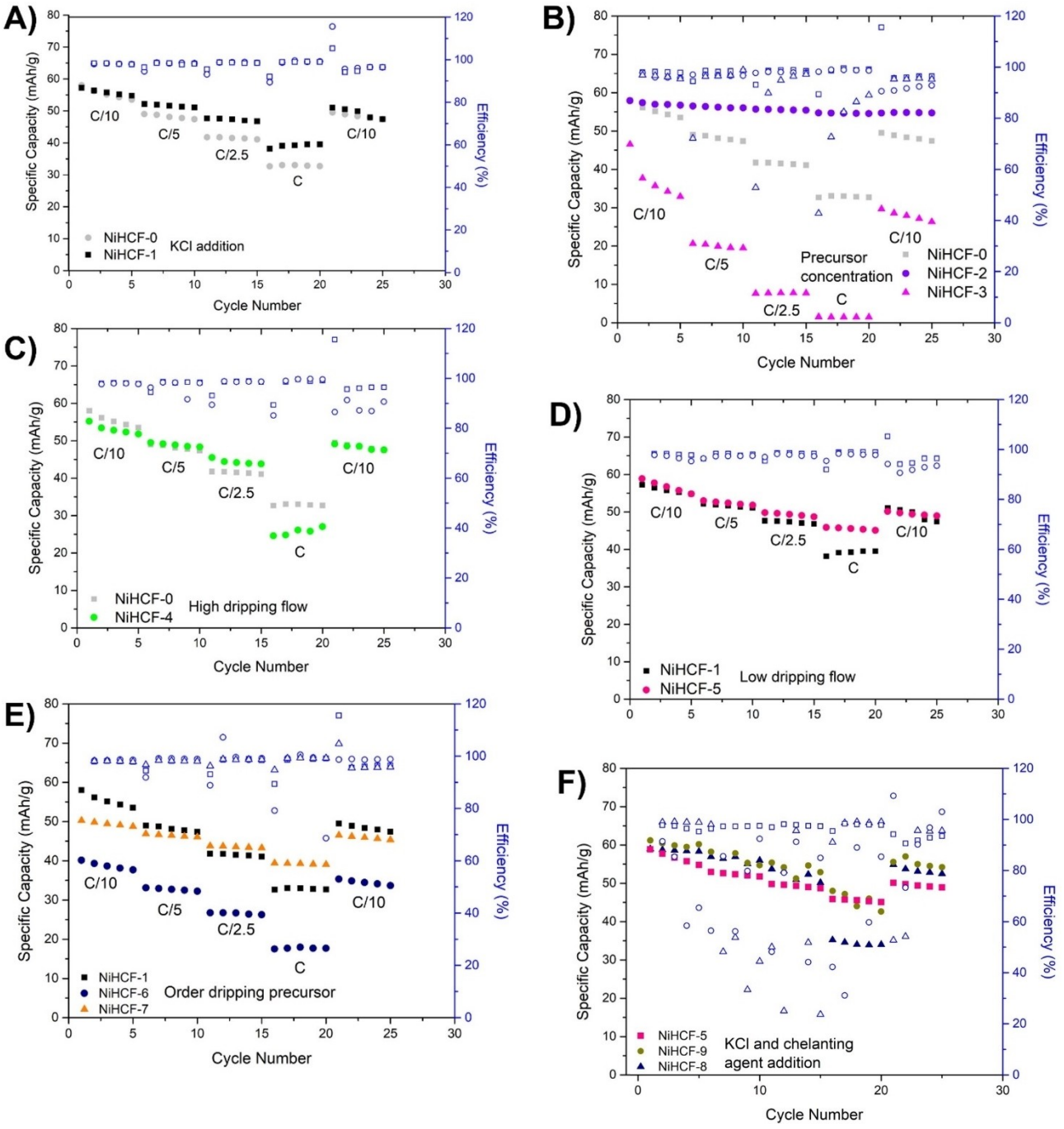

Figure 5. Electrochemical performance of NiHCF samples synthesized as sodium cathode using 1 M NaClO4 EC: PC as electrolyte. Comparison between samples NiHCF-0 and NiHCF-1 (A), NiCHF-0, NIHCF-2 and NiHCF-3 (B), NiHCF-0 and NiHCF-4 (C), NiHCF-1 and NiHCF-5 (D), NiHCF-1, NiHCF-6 and NiHCF-7(E) and NIHCF-8 and NIHCF-9 (F).

The electrochemical performance was highly affected by the precursor addition order (samples NiHCF-1, NiHCF-6, and NiHCF-7, Figure 5E and S.6) because such a parameter is critical for the dimension of the particles; indeed, sample NiHCF-6, having larger particle, showed a poor electrochemical performance, providing just 15 mAh/g at C-rate. The electrochemical behavior of sample 6 was considerably superior at a fast C-rate, with a half-capacity fading than sample NiHCF-1 and lower polarization, probably related to the lower aggregation of particles.

The use of a chelate agent as a precursor had a significant impact on the electrochemical performance of the materials, reaching the superior capacity delivered at low current densities (Figure 5F and S7), around 60 mAh/g, equivalent to 82% of the theoretical value; however, the capacity fading at faster C-rates was higher than for sample 5, which did not contain EDTA, yet

the capacity delivered was very similar since the higher Fe content of the sample based on EDTA synthesis. The worst performance at a faster C-rate could be attributable to the larger particle sizes caused by the slow nucleation.

Another key parameter for the potential implementation of these types of batteries is their cycling stability. It was analyzed by prolonged cycling at a rate equivalent to C/5 (Figure S8). Some materials showed poor capacity retention upon cycling, providing just ≈10 mAh/g after 100 cycles (samples NiHCF-6, 7, and 3). There was another set of samples with limited stability, reaching a capacity close to ≈30 mAh/g (samples NiHCF-1, 5, and 8), equivalent to approximately ≈50% of the theoretical capacity. A third group of samples showed a less severe capacity decay, delivering in the range of ≈40 mAh/g (NiHCF-9 and 0, 50–60% of theoretical values) or ≈50 mAh/g (NiHCF- 4, 80% theoretical value). On the other hand, sample NiHCF-2, based on a ratio $NiSO_4$:$K_4Fe(CN)_6$ equal to 5:1, showed impressive capacity retention, providing 95.1% of the theoretical capacity after 100 cycles, similar to the best NiHCF-based sodium batteries reported in the literature.[1,24,31,34]

Conclusions

The synthesis process of the NiHCF, a member of the Prussian Blue Analogue family, has been studied in detail. The synthesis is based on an easy coprecipitation method employing two precursors where different parameters can be modified, such as the nature and composition of the precursor, the addition of KCl, the presence of a chelating agent (EDTA), their concentrations, the order, or the flow rate of their addition. The effects of these synthesis conditions on the samples' composition, morphology, and electrochemical performance were analyzed, revealing the parameters' interrelation. For example, reducing the presence of vacancies by adding EDTA and KCl would have a beneficial impact on the electrochemical performance at a low scan rate. However, in this case, the Na^+ (de−)insertion kinetics are slower than those of EDTA-free samples because of their larger particle size. Unlike current opinion in the scientific community, where reducing the presence of vacancies by the addition of a chelating agent is the mainstream to reach superior sodium cathodes, we have demonstrated here that other parameters could play a similar role – medium flow rate, presence of KCl, low agglomeration – providing superior C-rate performances at similar compositions. This study has also revealed the crucial role of precursor concentrations (synthesis NiHCF-2). An excess of potassium hexacyanoferrate (III) allowed synthesizing the material with the best electrochemical performance because of its low vacancy/water level – in the range of chelate-based materials reported in the literature but without distortion from the traditional face-centered cubic structure. We think this synthesis route opens new ways for exploring alternative approaches based on excess of Fe-based precursor. This study also proved that for improving the electrochemical performance of NiHCF as a sodium cathode, a holistic analysis of sample properties – vacancy level, particle size, agglomeration, and iron oxidation state – is vital, as all these parameters are interconnected. We believe that this analysis could contribute to developing superior sodium cathodes based on Prussian Blue Analogues.

Experimental Section

Synthesis of $K_xNi[Fe(CN)_6]_y \cdot zH_2O$

A coprecipitation method modifying critical synthesis conditions was used. The initial synthesis procedure refers to the material called NiHCF-0, which is considered the benchmark material. 100 ml of 0.1 M nickel sulfate (Precursor A) and 0.1 M potassium hexacyanoferrate (III) (Precursor B) solutions were dropwise added to 60 ml of deionized water with continuous nitrogen flow and stirring at 60 °C. Once the coprecipitation was finished, the product was aged for 12 hours at room temperature. The precipitate was filtered and washed using a vacuum pump and a 0.2 μm porous membrane (CytivaTM). Finally, the material obtained was dried at 100 °C in a vacuum oven for 12 hours. Table 1 summarizes the different synthesis parameters used for each NiHCF batch. NiHCF-0 refers to an initial synthesis with standard conditions. The parameters modified for the rest of the synthesis concerning this initial procedure are shown in Table 1. Those parameters not indicated in Table 1 (temperature, stirring, and N_2 flow) remained equivalent for all the syntheses.

Structural Characterization

X-ray diffraction (XRD) measurements were carried out with a D8 Discover A diffractometer (Bruker) with a LynxEye detector and monochromatic Cu–Kα radiation (λ = 1.5406 Å). The diffractogram was measured from the 5° to 60° (2Θ) range, with a size of 0.02° per step with a rate of 16 s. The elemental composition was obtained by a combination of X-ray fluorescence (FRX) (Rigaku, Primus IV) and Thermo-gravimetric analysis (TGA). A TGA/DSC 1 STAR system (Mettler Toledo) was employed from 30° to 500 °C, with a ramp of 10 °C per minute under a nitrogen flow of 100 mLs^{-1}. Scanning electron microscopy (SEM) images were obtained using a Helios Nanolab 650 (FEI Europe B.V.)

Electrochemical Measurements

The electrochemical characterization was performed using a coin cell (CR2032). The cathode was prepared by coating NiHCF slurry over carbon-aluminum paper (Gelon Lib. Co. Ltd.) using a doctor blade process. The slurry was compounded by a mixture of active material (NiHCF), Carbon Black (SPC, Tymcal), and polyvinylidene difluoride (Sigma Aldrich) mixed with NMP (Sigma-Aldrich) in 80:10:10 weight proportions, prepared in an Ultra Turrax (T25 digital Ultra-Turrax). The samples were dried in a vacuum oven at 60 °C for 12 hours. Then, 12 mm diameter electrodes were die-cut and weighed, obtaining a mass loading of ≈1.5 $mgcm^{-2}$. The cell assembly followed the typical sequence: positive case, cathode, separator and electrolyte, anode, spacer, spring, and negative case. The separator was cellulose paper (Sarl Prat Dumas), and a 1 M $NaClO_4$ solution in EC: PC was employed as an electrolyte. The assembly was made inside a Glove Box (M-Braun 150 model) with water and oxygen contents lower than one ppm. Electrochemical measurements were performed using a Naware BTS 4000 potentiostat or an EC-Biologic potentiostat MPG-2. The specific capacity values and C-rate of the Na ion coin cell were calculated based on the active material loading in the electrode and the molecular composition of each sample. A value of 1 C rate means that at the

applied current, the material will be fully oxidized/reduced in 1 hour. Similarly, C/10 would mean that for that applied current, it takes ten hours to complete the oxidation/reduction. A potential range from 2.7 V to 3.95 V vs. sodium was employed.

Acknowledgements

The authors are grateful to the technical staff from the Instituto Químico para la Energía y el Medioambiente (IQUEMA) and Servicios Centrales de Apoyo a la Investigación (SCAI) of Málaga University. The authors thank the support of the Junta de Andalucia through funding the projects "Program EMERGIA Emergía_0153" and "Project Excel_00330", as well as to the Ministry of Science, Innovation, and Universities through the projects "TED20213129314 A-100" and PID2022-142391OA-100, and the grant RYC2022-037564 founded by the MCI/AEI// 10.13039/501100011033 and European Union NextGenerationEU/PRTR, FEDER a way of making Europe and the FSE invest in your future. Funding for open access charge: Universidad de Córdoba / CBUA

Conflict of Interests

The authors declare no conflict of interest.

Data Availability Statement

The data that support the findings of this study are available from the corresponding author upon reasonable request.

Keywords: Sodium-ion batteries · Prussian blue analogues · NiHCF · Synthesis methods · Electrochemistry

[1] Y. Xu, J. Wan, L. Huang, M. Ou, C. Fan, P. Wei, J. Peng, Y. Liu, Y. Qiu, X. Sun, C. Fang, Q. Li, J. Han, Y. Huang, J. A. Alonso, Y. Zhao, *Adv. Energy Mater.* **2019**, *9*, 1803158.
[2] Energy Storage - Underpinning a decarbonised and secure EU energy system. Brussels, 14.3.2023 SWD(2023) 57.
[3] W. Lv, Z. Wang, H. Cao, Y. Sun, Y. Zhang, Z. Sun, *ACS Sustain. Chem. Eng.* **2018**, *6*, 1504–1521.
[4] M. S. Palagonia, D. Brogioli, F. L. Mantia, *J. Electrochem. Soc.* **2017**, *164*, E586.
[5] C. D. Wessells, S. V. Peddada, R. A. Huggins, Y. Cui, *Nano Lett.* **2011**, *11*, 5421–5425.
[6] V. Carnero-Roldán, A. Licarí, M. Castillo-Rodriguez, F. La Mantia, R. Trócoli, *Electrochim. Acta* **2024**, *490*, 144237.
[7] M. S. Chae, J. W. Heo, H. H. Kwak, H. Lee, S.-T. Hong, *J. Power Sources* **2017**, *337*, 204–211.
[8] R. Trócoli, R. Houdeville, C. Frontera, S. Vincent, J. M. Garcia Lastra, M. R. Palacín, *ChemSusChem* **2024**, *17*, e202301224.
[9] R. Trcoli, *ChemSusChem* n.d. DOI: 10.1002/cssc.201403143.
[10] G. Kasiri, R. Trócoli, A. Bani Hashemi, F. La Mantia, *Electrochim. Acta* **2016**, *222*, 74–83.
[11] R. Trócoli, P. Parajuli, C. Frontera, A. P. Black, G. C. B. Alexander, I. Roy, M. E. Arroyo-de Dompablo, R. F. Klie, J. Cabana, M. R. Palacín, *ACS Appl. Energy Mater.* **2022**, *5*, 11964–11969.
[12] R. Trócoli, G. Kasiri, F. La Mantia, *J. Power Sources* **2018**, *400*, 167–171.
[13] Y. You, X.-L. Wu, Y.-X. Yin, Y.-G. Guo, *Energy Environ. Sci.* **2014**, *7*, 1643–1647.
[14] S. Yu, Y. Li, Y. Lu, B. Xu, Q. Wang, M. Yan, Y. Jiang, *J. Power Sources* **2015**, *275*, 45–49.
[15] C. D. Wessells, S. V. Peddada, M. T. McDowell, R. A. Huggins, Y. Cui, *J. Electrochem. Soc.* **2011**, *159*, A98–A103.
[16] F. Scholz, A. Dostal, *Angew. Chem. Int. Ed. Engl.* **1996**, *34*, 2685–2687.
[17] J. Song, L. Wang, Y. Lu, J. Liu, B. Guo, P. Xiao, J.-J. Lee, X.-Q. Yang, G. Henkelman, J. B. Goodenough, *J. Am. Chem. Soc.* **2015**, *137*, 2658–2664.
[18] K. Hurlbutt, S. Wheeler, I. Capone, M. Pasta, *Joule* **2018**, *2*, 1950–1960.
[19] R. Y. Wang, B. Shyam, K. H. Stone, J. N. Weker, M. Pasta, H. Lee, M. F. Toney, Y. Cui, *Adv. Energy Mater.* **2015**, *5*, 1401869.
[20] G. Du, H. Pang, *Energy Storage Mater.* **2021**, *36*, 387–408.
[21] M. Fiore, S. Wheeler, K. Hurlbutt, I. Capone, J. Fawdon, R. Ruffo, M. Pasta, *Chem. Mater.* **2020**, *32*, 7653–7661.
[22] R. Wei, X. Zhai, H. R. Tinker, P. He, C. A. F. Nason, Y. Han, V. Celorrio, G. Sankar, M. Zhou, Y. Xu, *Adv. Funct. Mater.* **2023**, *33*, 2308227.
[23] X. Han, D. Zhang, Z. Xie, Y. Xing, *ACS Appl. Nano Mater.* **2023**, *6*, 22333–22343.
[24] J. Peng, M. Ou, H. Yi, X. Sun, Y. Zhang, B. Zhang, Y. Ding, F. Wang, S. Gu, C. A. López, W. Zhang, Y. Liu, J. Fang, P. Wei, Y. Li, L. Miao, J. Jiang, C. Fang, Q. Li, M. T. Fernández-Díaz, J. A. Alonso, S. Chou, J. Han, *Energy Environ. Sci.* **2021**, *14*, 3130–3140.
[25] L. Xue, Y. Li, H. Gao, W. Zhou, X. Lü, W. Kaveevivitchai, A. Manthiram, J. B. Goodenough, *J. Am. Chem. Soc.* **2017**, *139*, 2164–2167.
[26] G. Małecki, A. Ratuszna, *Powder Diffr.* **1999**, *14*, 25–30.
[27] L. Zhang, L. Chen, X. Zhou, Z. Liu, *Sci. Rep.* **2015**, *5*, 18263.
[28] M. Avila, L. Reguera, J. Rodríguez-Hernández, J. Balmaseda, E. Reguera, *J. Solid State Chem.* **2008**, *181*, 2899–2907.
[29] S. Adak, L. L. Daemen, M. Hartl, D. Williams, J. Summerhill, H. Nakotte, *J. Solid State Chem.* **2011**, *184*, 2854–2861.
[30] C. D. Wessells, R. A. Huggins, Y. Cui, *Nat. Commun.* **2011**, *2*, 550.
[31] X. Wu, C. Wu, C. Wei, L. Hu, J. Qian, Y. Cao, X. Ai, J. Wang, H. Yang, *ACS Appl. Mater. Interfaces* **2016**, *8*, 5393–5399.
[32] V. D. Ivanov, *Ionics* **2020**, *26*, 531–547.
[33] S. L. Kessel, R. M. Emberson, P. G. Debrunner, D. N. Hendrickson, *Inorg. Chem.* **1980**, *19*, 1170–1178.
[34] L. Deng, J. Qu, X. Niu, J. Liu, J. Zhang, Y. Hong, M. Feng, J. Wang, M. Hu, L. Zeng, Q. Zhang, L. Guo, Y. Zhu, *Nat. Commun.* **2021**, *12*, 2167.
[35] M. B. Zakaria, T. Chikyow, *Coord. Chem. Rev.* **2017**, *352*, 328–345.
[36] C. Ding, Z. Chen, C. Cao, Y. Liu, Y. Gao, *Nano-Micro Lett.* **2023**, *15*, 192.
[37] T. Utsunomiya, O. Hatozaki, N. Yoshimoto, M. Egashira, M. Morita, *J. Power Sources* **2011**, *196*, 8675–8682.
[38] W. M. Seong, K.-Y. Park, M. H. Lee, S. Moon, K. Oh, H. Park, S. Lee, K. Kang, *Energy Environ. Sci.* **2018**, *11*, 970–978.
[39] R. Trócoli, A. Morata, C. Erinmwingbovo, F. La Mantia, A. Tarancón, *Electrochim. Acta* **2021**, *373*, 137847.

Manuscript received: May 3, 2024
Revised manuscript received: October 22, 2024
Accepted manuscript online: October 22, 2024
Version of record online: November 19, 2024